Coupled Inductors for Fast-Response High-Density Power Delivery: Discrete and Integrated

Charles R. Sullivan
Thayer School of Engineering at Dartmouth, Hanover, NH, USA
Minjie Chen
Department of Electrical Engineering and Andlinger Center for Energy and the Environment, Princeton Univ., Princeton, NJ, USA

Abstract Multiphase interleaved buck converters benefit from coupling inductors between phases. The coupling fundamentally alters the trade-offs between ripple current, loss, energy storage, and transient response, enabling improvements in one or more of these aspects without compromises in the others. Coupled-inductor buck converters implemented with discrete or integrated switches, controls, and inductors have become a standard technique for power delivery applications. This paper reviews developments in this technology across many applications and shows how a simplified analysis approach can offer added design insight for both magnetics designers and circuit designers.

1 Introduction

In a basic buck converter, the choice of inductance value entails several important trade-offs. A larger inductance reduces current ripple in the inductor, and thus reduces conduction losses in the inductor and switches. It also reduces ripple current in the output capacitor, and thus provides lower output voltage ripple. However, it also slows the response time: it reduces the speed at which the converter can respond to changes in load current or to changes in commanded output voltage. And it requires higher energy storage, thus requiring the inductor to physically larger and/or have higher loss.

An early development in power converter designs to overcome this limitation was the use of multiphase interleaved converters: multiple parallel converters, operated out of phase, i.e., with a delay of T/M between the switching cycles of adjacent phases, where T is the period and M is the number of phases [1–4]. When the phase currents are combined at the output, they provide partial cancellation of the ripple current. This results in lower ripple voltage at the output, or, for a given tolerable level of ripple, it allows using smaller inductors for faster response, smaller size, and lower loss. However, the smaller inductor values result in higher ripple in the individual phase currents, and that higher current flows in in the inductors and the switches, increasing loss.

Coupling the inductors between phases, if done properly, can extend most of the ripple reduction achieved in the output through the individual phase currents. This allows side-stepping the compromise between small and large inductor values and achieving the benefits of both [5–11]. Although some early versions of this coupled only two phases with moderate coupling and provided limited ripple-reduction benefits, it was shown in [6, 7] that strong coupling can be achieved while keeping energy storage low and thus achieving high performance with compact, low-loss components, and that the benefits can be extended to coupling any number of phases in one magnetic structure.

The benefits of highly coupled multiphase implementations can include reduced ripple leading to reduced loss in switches, inductor windings, and output capacitors; reduced energy storage requirements for inductors leading to reduced loss, cost, and size; faster transient response (and thus more stable output voltage during transients), and reduced output capacitor size. The designer can choose to prioritize the benefits in some of these parameters while holding others fixed, or to achieve more modest improvements in all of them [6].

Some of these benefits, including the reduced inductor physical size and reduced output capacitor size requirement, make coupled inductors attractive for chip-scale microfabricated in-package or on-die implementation [12–18]. As reviewed in [19–21], microfabrication of magnetic components poses many challenges, although it also offers opportunities that have not yet been fully realized. Coupled inductors provide ways to address some of these challenges, but also pose challenges of their own.

In this paper, we first discuss modeling approaches for multi-winding coupled inductors and multiphase converters using them. We show that the analysis can be simplified by considering the ripple reduction in terms of two parameters that quantify the effect of multiphase interleaving and the effect of coupling, offering additional insight and as well as facilitating design calculations, as discussed in more detail in [22]. Next we apply this background to examine the approaches that can be and have been used to develop on-die and in-package microfabricated coupled inductors.

2 Multiphase Coupled Inductor Structures and Models

For a two-phase coupled inductor, the physical structure can be the same as a transformer, and the model can be a standard T or Pi transformer model. For a multiphase inductor, the preferred structure configures the windings on parallel core paths, for example, as shown in Fig. 1 [6–8, 10, 11]. There are two key reasons for using this configuration. The first is that this topology tends to equalize the ac current in the different windings when a high-permeability core is used, approaching forcing exactly equal currents in the limit when the core reluctance becomes negligible [6, 22]. An additional essential feature of this configuration is that the dc flux in a given leg resulting from that leg's winding excitation is mostly cancelled by the dc flux in the same leg from generated by the other windings when all are excited with equal dc currents. Thus, it is possible to use an ungapped high permeability core to achieve strong coupling without magnetic saturation.

A magnetic circuit model of the structure in Fig. 1 is shown in Fig. 2. Although there is no explicit leakage path shown in Fig. 1, the flux leakage between the top and bottom bar is important to the operation of this structure in a typical circuit, and is modeled by the four leakage reluctances, $\mathcal{R}_l$. If the core has sufficiently high permeability, or if the top and and bottom bars of the core have sufficiently large cross sectional area, we can neglect the reluctance of those parts of the core, $\mathcal{R}_t$, resulting in the model in Fig. 3. In this model, each winding leg has a reluctance $\mathcal{R}_L$. The full model in Fig. 2 may be used in simulation, using the magnetic circuit model directly [6] or an equivalent electrical circuit or inductance matrix model [22], but the simpler model still captures the main features of the circuit behavior and can be useful for understanding the circuit and magnetics design issues.

For simulation of a full converter circuit and for understanding circuit operation, it is useful to convert this magnetic circuit model to an electrical circuit model. As explained in [22], the topology of the electrical circuit model arising directly from Fig. 3 is the topological dual, with reluctances replaced by inductors as shown in Fig. 4. This model is attractive not only for its simplicity, but also because each inductor in the model corresponds to a specific physical part of the structure. The magnetic flux in each inductor is linearly related to the magnetic flux in the corresponding part

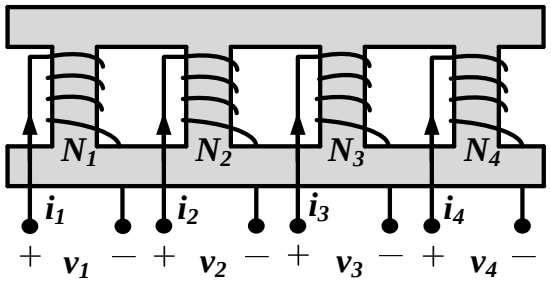

Figure 1: Multiwinding coupled inductor with a ladder core. The windings' magnetic paths are in parallel and thus have approximately equal MMF and per-turn voltages that sum to zero.

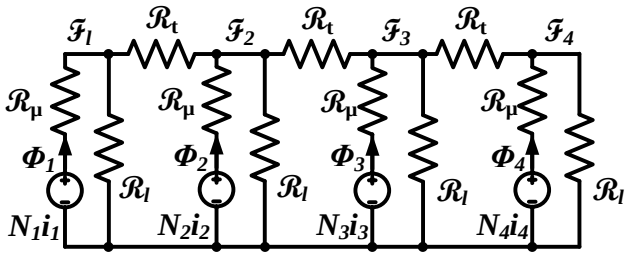

Figure 2: Magnetic circuit model of the ladder structure in Fig. 1. Labeled values $\mathcal{R}$ are reluctance values.

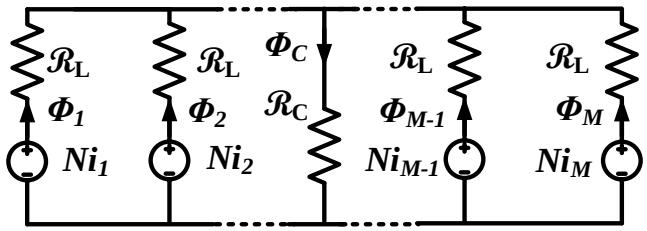

Figure 3: Simplified magnetic circuit model of the structure in Fig. 1, neglecting $\mathcal{R}_t$ and lumping all the leakage paths into one central leakage reluctance $\mathcal{R}_C$

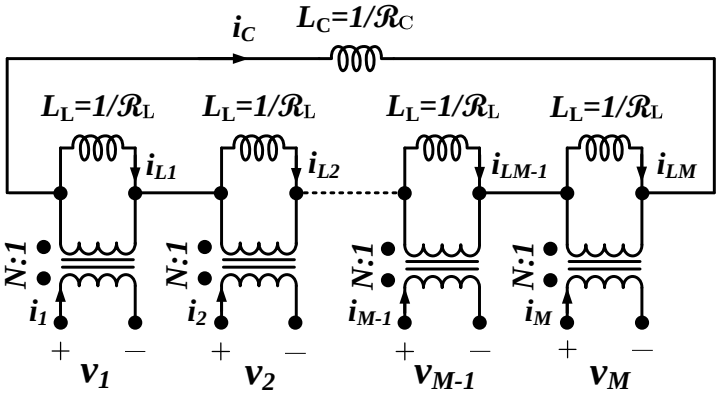

Figure 4: Inductance dual model of the magnetic circuit in Fig. 3. $1/\mathcal{R}_C$ and $1/\mathcal{R}_L$ represent the inductive elements of the combined leakage paths (C) and the wound core legs (L). In SPICE simulations with ideal transformers, the ac components of i_C and i_L are linearly related to the ac components of Φ_C and Φ_L in the leakage paths and the wound legs, respectively.

of the core, and this facilitates modeling of non-ideal magnetic behavior including core losses and saturation [22].

For gaining circuit intuition, a multiwinding transformer model can also be attractive. There are several approaches to this. Fig. 5 shows one example using an ideal current equalizing trans-

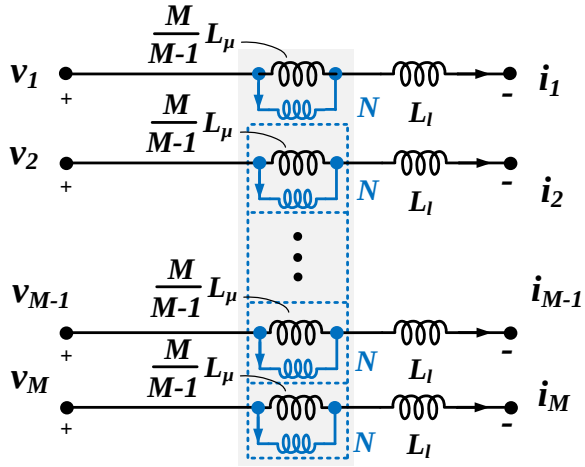

Figure 5: Multiwinding transformer model of the magnetic circuit in Fig. 3 implemented with an ideal current equalizing transformer (in blue). The ideal current equalizing transformer equalizes the current of all blue windings and forces the sum of the voltages of all windings to be zero.

former [22, 23]. This model includes a magnetizing inductance in parallel with each each winding of the ideal current equalizing transformer and a leakage inductance L_l in series. The turns ratio of the ideal current equalizing transformer is $\{1 : 1 : ... : 1\}$, assuming equal numbers of turns N in each physical winding. The individual magnetizing inductances have a value $\frac{M}{M-1}L_\mu$, where L_μ is defined by analogy to magnetizing inductance in a two-winding transformer as $L_\mu = L_S - L_l$ where L_S is the self inductance (measured on one winding of the structure with the others open-circuited) and is also equal to the self inductance in the inductance matrix equation. To write this model in the form of an inductance matrix, we also need the mutual inductance $L_M = -\frac{1}{M-1}L_\mu$.

The behavior of the models in Figs. 3, 4 and 3 are all identical—they are only alternative ways of representing this behavior in a circuit. There are additional options discussed in [22] that also result in identical behavior, but these three are our preferred representations.

3 Analysis and Performance of Multiphase Coupled-Inductor Buck Converter

By coupling multiple inductors of a multiphase buck converter with a single high-permeability magnetic core, one can significantly reduce the current ripple in each of the phase in order to reduce the conduction loss in switches, windings, and printed circuit board traces. One can, of course, achieve, the same ripple reduction in a single-phase or multiphase uncoupled design by using a larger inductor value, but this has two important disadvantages: It increases the energy storage, and thus increases the size and loss of the inductor. And it slows the transient response. Since these two effects scale together, we focus on considering ripple reduction for a fixed transient response impedance, and thus show the improvement available through coupling without the disadvantages of increasing inductance in the absence of coupling [22]. Although this choice is to some extent arbitrary, it is essential to make a careful and deliberate choice of what to hold fixed while varying the amount of coupling. The reader is cautioned to apply skepticism to analyses in the literature that vary coupling without a clear statement of what is held fixed as coupling is varied, and why.

Even without coupling, the use of multiple phases can reduce

ripple through partial cancellation at the output by multi-phase interleaving [1–3]. To compare an uncoupled multiphase converter to a single-phase converter, we apply the constraint of equal transient response. With M phases, the reaction of the system to a perturbation in duty cycle across all phases, or to simply switching all phases high or low in a more urgent situation, is an equal perturbation applied to all M inductors, effectively connected in parallel. Thus, for equal transient response, the parallel combination of M inductors in the multiphase circuit should be equal to the value of the inductor used in the single-phase circuit: $L_{1\phi} = L_{M\phi}/M$, where $L_{M\phi}$ is the per-phase uncoupled inductor value used in an M-phase circuit. With this choice, the absolute ripple-current amplitude in each phase is lower than the total ripple current in the single-phase converter by a factor of $1/M$. The dc current in each phase is also lower than the overall dc current by the same factor, so each inductor of the M-phase design has the same current ripple ratio as the inductor with the same inductance in a single-phase design.

In the multi-phase converter, the total output capacitor current ripple amplitude, after partial cancellation of the ripple current when the individual phase currents are combined, is reduced compared to the ripple in the single-phase converter by a factor that depends on the relationship between the duty ratio and the number of phases. As the way the phases interact depends on how many phases are energized simultaneously, it is convenient to introduce an integer index k such that $\frac{k}{M} \leq D < \frac{k+1}{M}$. In terms of k, duty ratio D and number of phases M, the output ripple of an interleaved uncoupled multiphase buck converter is reduced relative to that of a single-phase converter with the same response time by a factor

$$\Gamma \stackrel{\text{def}}{=} \frac{\Delta i_o^{M\phi}}{\Delta i_o^{1\phi}} = \frac{(k+1-DM)(DM-k)}{(1-D)DM^2}, \tag{1}$$

where we use the notation $\Delta i_o^{M\phi}$ to indicate peak-to-peak current ripple amplitude with the subscript o indicating the output, or overall ripple after the phase currents are combined, and the superscript $M\phi$ indicates an M-phase converter. Γ quantifies the benefits of interleaving for output current ripple reduction.

Fig. 6 plots Γ as a function of M and D. Γ decreases as M increases. When the duty cycle is near an integer multiple of $1/M$, Γ approaches 0, indicating fully cancelled output current ripple. The advantage of coupling is that some of this benefit of output current ripple reduction can be extended to the ripple in each phase, and indeed, practical designs can approach the full reduction factor given by (1) with strong coupling.

We wish to consider coupled designs in the same framework of fixing transient response and varying other parameters, so we first evaluate the transient response. We can do this based on any of the models, considering either a small-signal perturbation to D or the large signal response with all phases switch high or low, with equivalent results in all cases [22]. The result is that impedance of the whole structure to this common-mode excitation is the impedance of the parallel combination of all the leakage inductances, L_l/M. Perhaps the most intuitive way to understand this is to consider the transformer model (Fig. 5) with all of the (+) terminals connected together and all of the (-) terminals connected together. The transformer equation requires all of the transformer winding voltages to sum to zero, and by symmetry, the only way for this to happen is with zero voltage across all of them, and thus zero voltage across the magnetizing inductances. The transformer portion of the model is transparent to this common mode

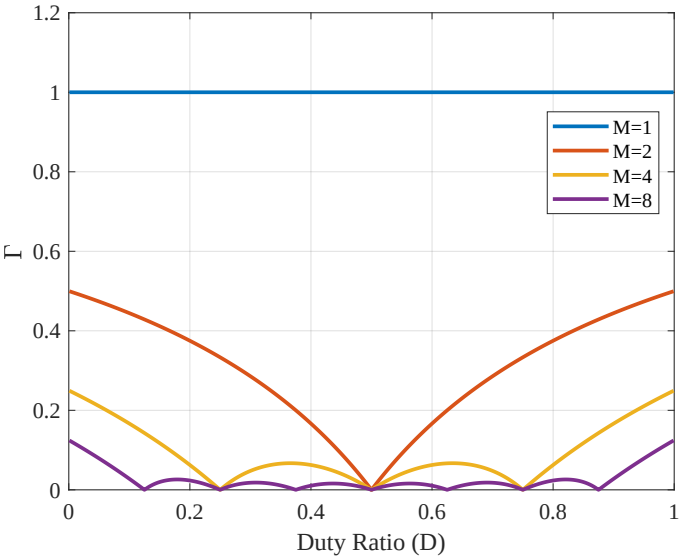

Figure 6: Output current ripple reduction factor (Γ) for an M-phase interleaved buck converter with duty ratio D. Γ quantifies the benefit of interleaving for output current ripple reduction in multiphase buck converters, whether coupled or not.

excitation, and the impedance is just that of the leakage inductances. Thus, the leakage inductance L_l determines the transient impedance [22, 24]. For ripple comparisons, we want to consider holding the leakage inductance fixed as we vary the coupling.

The steady-state ripple in the coupled case has been calculated in many different papers, with equivalent results, even though different formulations are used, as discussed in more detail in [22], where, to simplify the calculations, we define a phase ripple current reduction ratio γ as

$$\gamma \stackrel{\text{def}}{=} \frac{\Delta i_p^{cp}}{\Delta i_p^{noncp}}, \tag{2}$$

with the inductance value in the uncoupled case equal to the leakage inductance of the coupled system for equal transient response. We use the superscripts cp or $noncp$ to indicate the coupled or uncoupled cases. The resulting phase current ripple amplitude is the standard buck converter ripple, reduced by the factor γ:

$$\Delta i_p = \gamma \frac{V_{OUT}(1-D)T}{L_l}, \tag{3}$$

where we again use the notation Δi to indicate peak-to-peak ripple, and the subscript p indicates the ripple in the winding of one of the M phases. The superscript $M\phi$ is dropped because the subscript p only applies when there are multiple phases.

To find γ or similar performance metrics as a function of the magnetic structure design, various papers in the literature use different parameters to describe the degree of coupling. We use a reluctance ratio $\beta \stackrel{\text{def}}{=} M\mathcal{R}_C/\mathcal{R}_L$ which is the ratio of combined leakage reluctance to the parallel combination of all the wound leg reluctances, partly because this directly describes the impact of the physical structure on performance, and partly because, it leads to a simplified calculation of γ in terms of Γ [22]:

$$\gamma = \frac{\frac{1}{\beta} + \Gamma}{\frac{1}{\beta} + 1} = \frac{1 + \beta \cdot \Gamma}{1 + \beta}. \tag{4}$$

As illustrated in Fig. 7, this equation shows how the benefits of multiphase interleaving in reducing the output current ripple (Γ) are extended to phase current ripple reduction by the coupling factor (β). As coupling increases (a high value of β), the ripple

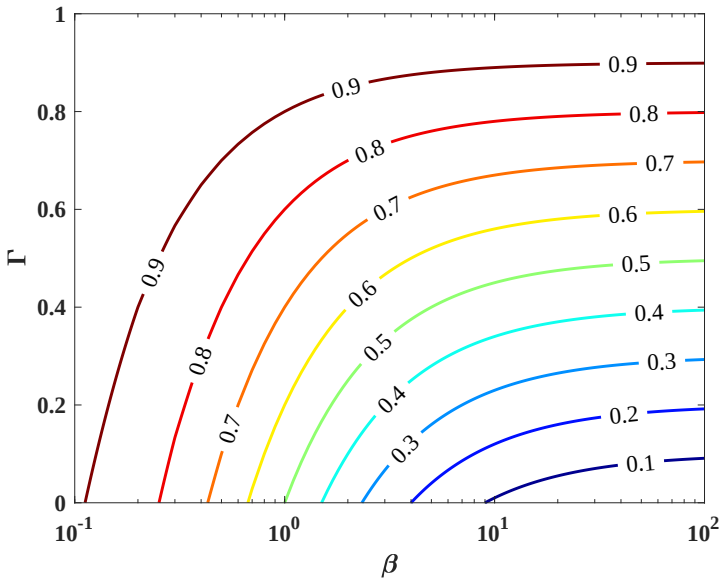

Figure 7: Contours of phase current ripple reduction factor (γ) for a multiphase coupled buck converter as a function of the output current ripple factor (Γ) and coupling coefficient (β). As β increases, γ approaches Γ, indicating that coupling extends the output current ripple improvement achieved through multiphase interleaving to the individual phase currents.

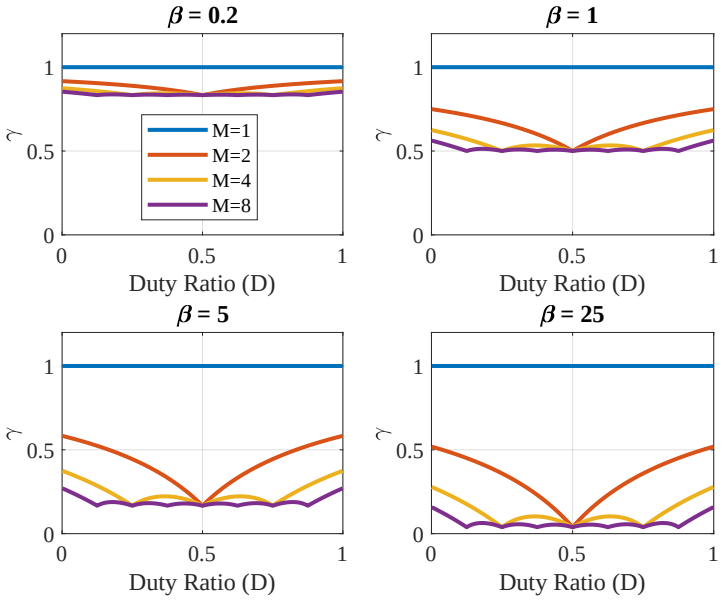

Figure 8: Phase current ripple reduction factor γ for a multiphase coupled buck inductor as a function of the duty ratio (D) for various numbers of phases (M) and reluctance ratios ($\beta = M\mathcal{R}_C/\mathcal{R}_L$). A lower γ indicates more winding current ripple reduction. A high β indicates strong coupling, and a low β indicates weak coupling.

reduction achieved in the phases approaches the ripple reduction in the combined output, Γ. This can be intuitively understood from the transformer model in Fig. 5: as coupling increases and L_μ becomes large, the transformer enforces equal current ripple in all phases, equal to the ripple that would be seen in the output after they all combine. As the coupling decreases, the result strays from this ideal. For small Γ, such as at duty cycle near an integer multiple of $1/M$, it approaches $\gamma = 1/(1+\beta)$. Fig. 8 plots γ for a range of D, M, and β. γ is always between zero and one, with a smaller γ being better, indicating reduced ripple, or, if ripple is held fixed, an opportunity to reduce inductance to make the

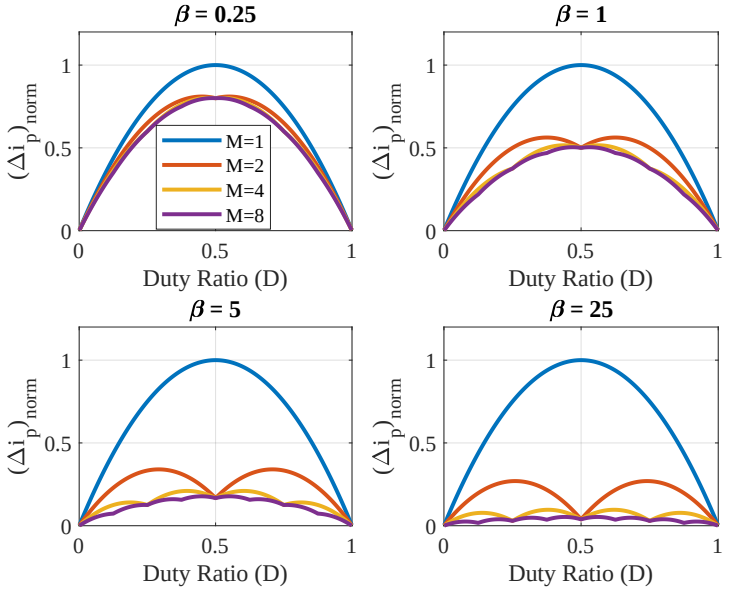

Figure 9: Normalized winding current ripple $(\Delta i_p)_{norm}$ for a multiphase coupled buck inductor as a function of the duty ratio (D) for various numbers of phases (M) and reluctance ratios ($\beta = M\mathcal{R}_C/\mathcal{R}_L$). A lower $(\Delta i_p)_{norm}$ indicates smaller absolute winding current ripple. A high β indicates strong coupling, and a low β indicates weak coupling.

Table 1: Key Parameters for Multiphase Coupled Buck Converters

Coupling Parameter	$\beta = \frac{M\mathcal{R}_C}{\mathcal{R}_L} = \frac{M}{M-1}\frac{L_\mu}{L_l} = \frac{-M\cdot L_M}{L_S+(M-1)L_M}$
Output Ripple Reduction	$\Gamma = \frac{\Delta i_o^{M\phi}}{\Delta i_o^{1\phi}} = \frac{(k+1-DM)(DM-k)}{(1-D)DM^2}$
Phase Ripple Reduction	$\gamma = \frac{\Delta i_p^{cp}}{\Delta i_p^{nocp}} = \frac{1+\beta\Gamma}{1+\beta}$
Normalized Output Current	$(\Delta i_p)_{norm} = \frac{\Delta i_{cp,phase}}{\Delta i_{max,cp,phase}} = 4D(1-D)\gamma$

magnetic components smaller and speed up transient response. We can see that for sufficiently large β, the ripple reduction γ approaches Γ. For moderate β, if D is close to an integer multiple of $1/M$, the ripple reduction approaches $1/(1+\beta)$ as discussed above: for example, when $\beta = 1$ the curves all go to $1/2$ at integer multiple of $1/M$.

In practice, β can be increased by reducing $\mathcal{R}_L$, by using high permeability core material, reducing length of the legs, and increasing area of the legs. $\mathcal{R}_C$ is then adjusted to maintain the selected L_l to meet the transient requirements while maintain a small ripple. Trade-offs exist between core loss, saturation margin, energy storage requirements, and transient response. In an optimal design, the core loss, winding loss, efficiency, power density, and transient and steady-state performance are highly correlated and need to be jointly optimized for a given design specification. For example, the work in [6] uses such optimizations to show how coupling can reduce volume and loss while holding transient response fixed, or improve transient response while holding volume and loss fixed. The number of phases is also considered, and for the parameters used in that work, it is shown that 4 to 6 phases is preferred. With fewer phases, there is less of a benefit from coupling, whereas with more phases, general magnetics scaling trends [21] that lead to lower efficiency and power density with many small inductors kick in.

Short of a full optimization as in [6], a good strategy to design coupled inductors for multiphase buck converter is:

1. Selected a magnetic structure with $\mathcal{R}_L \ll \mathcal{R}_C$;

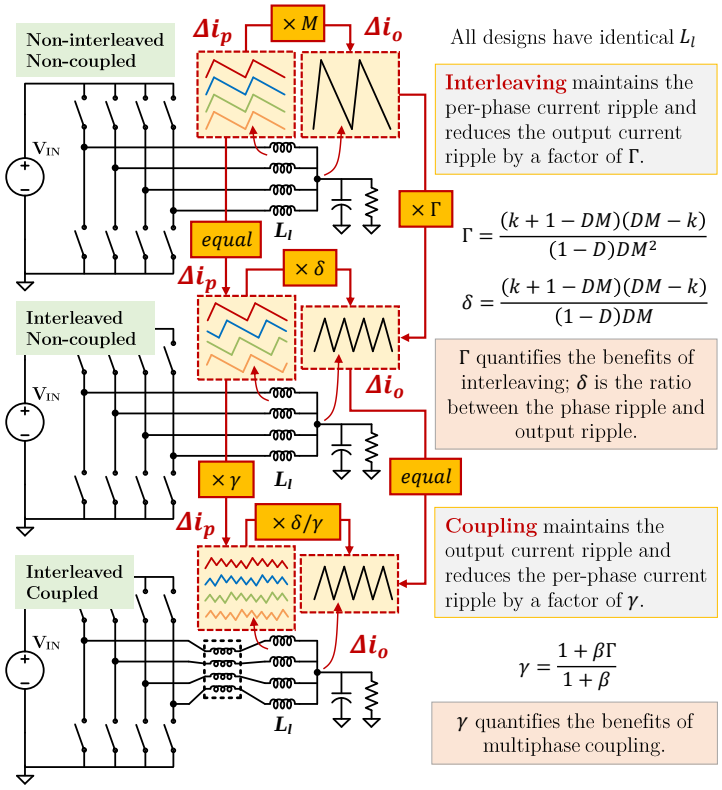

Figure 10: Summary of the key design parameters of a few multiphase buck converters with the same transient performance. Interleaving maintains the per-phase current ripple and reduces the output current ripple by a factor of Γ. Coupling extends the benefits of interleaving to phase current reduction, and reduces the phase current ripple by a factor of γ.

2. Choose an appropriate per-phase transient inductance (L_l) based on the tradeoff between transient response and the overall output voltage ripple, assuming that a high β will allow approaching a ripple reduction close the the ideal of $\gamma = \Gamma$.

3. Determine the required value of $\mathcal{R}_L + M\mathcal{R}_C$ based on the selected L_l and N.

4. Design the magnetic structure (material and geometry) to minimize $\mathcal{R}_L$ and adjust $\mathcal{R}_C$ to maintain the selected L_l. In choosing the geometry parameters, cosiderations include minimizing the loss and ensuring enough margin to avoid saturation under balanced excitation.

5. Evaluate the flux under the expected worst-case mismatch between phase currents. If this leads to saturation, add small gaps in the wound legs as necessary to accommodate the mismatch.

There is always parasitic inductance adding to L_l of the coupled inductor. When the targeted value of L_l is small, the parasitic inductance outside the transformer may provide a significant fraction of the necessary leakage inductance, thus providing an opportunity to reduce the required inductance and thus reduce the energy storage required in the magnetic structure and reduce its size. In some cases, the parasitic inductance may exceed the targeted value of L_l, and careful layout to reduce parasitic inductance may be needed.

The absolute value of the current ripple per-phase impacts the loss in the windings and switches. If D varies over a significant range in an application, it is useful to consider the worst-case absolute ripple for a given design, not just the ripple reduction ratio γ. The current ripple of each phase is

$$\Delta i_p = \gamma \frac{V_{IN} D(1-D)T}{L_l}. \tag{5}$$

A helpful way to consider this is to normalize it to the worst-case phase current ripple at $D = 0.5$ with no coupling,

$$\Delta i_p^{max} = \frac{V_{OUT} T}{2L_l} = \frac{V_{IN} T}{4L_l}, \tag{6}$$

resulting in the normalized current ripple:

$$(\Delta i_p)_{norm} \stackrel{\text{def}}{=} \frac{\Delta i_p}{\Delta i_p^{max}} = \gamma 4D(1-D) = \frac{1+\beta\Gamma}{1+\beta} 4D(1-D). \tag{7}$$

Fig. 9 plots this normalized current ripple across a range of D, M, and β. Both Figs. 9 and 8 illustrate the advantages of increasing the coupling and of increasing the number of phases. Fig. 8 directly shows how much benefit is provided at a given operating point, whereas Fig. 9 is useful for considering a range of operating points with different duty ratios, and assessing the ripple and ripple reduction at the worst-case point over that range.

Table 1 lists the key design parameters for multiphase coupled inductors. Fig. 10 illustrates the relationships among these parameters.

4 Microbrabricated Coupled Inductors

Despite recent progress, fabrication of on-die or in-package power magnetics with high efficiency and high power density remains difficult. This results from general characteristics of magnetics scaling that make high efficiency difficult to achieve in small sizes [21], as well as the specific technological challenges discussed in more detail in [19,20]. However as practical power converter switching frequencies increase, the power level that can be handled efficiently by small magnetic components goes up, and the advantages offered by high-performance thin-film magnetic materials, not available in bulk form, become more significant.

Although microfabricated coupled inductor design and fabrication entails many of the same considerations as uncoupled inductor design and fabrication, there are some aspects that are easier and some that are harder. A particular challenge in uncoupled inductors is the need for low-permeability magnetic materials or air-gaps in the magnetic path [19]. Coupled inductors can be configured to provide dc flux cancellation, allowing the use high high permeability materials such as CoZrTa and NiFe in a high-current application without the need to add air gaps to avoid saturation, making the use of these high-performance easily deposited materials feasible. On the other hand, the specific geometry requirements involved in coupling multiple phases add an additional complication to the topological challenges already involved in making any magnetic-core microfabricated magnetics.

Realizing the full potential of coupled inductors requires a closed, or nearly closed, flux path in a high-permeability magnetic core. Topologically, this requires that the winding and the core must constitute two interlinked loops. In some cases the conductor loop comprises multiple turns, although for low-voltage, high-current applications, the impedance is low enough that a single turn is optimal. In any case, interlinking the two requires at least three deposition steps: either the core or the winding can occupy just one layer, but the other needs to be deposited in two steps. Following the terminology of in [19,25], we call designs in the class

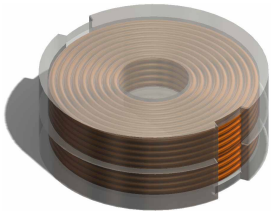

(a) Pot core

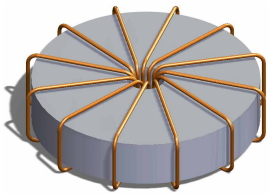

(b) Toroid

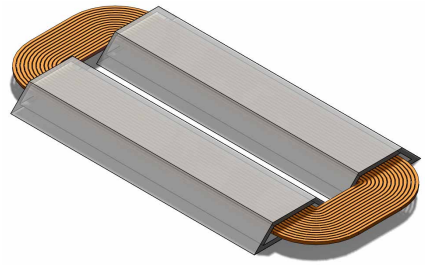

(c) 'Racetrack' thin-film pot core

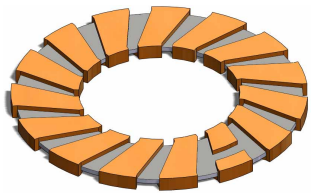

(d) Thin-film toroid

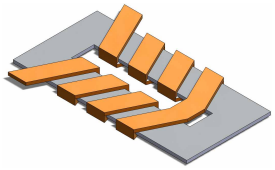

(e) Thin-film rectangular toroid

Figure 11: Classes of magnetic-core inductor and transformer geometries. The top row shows the conventional wire-wound geometries from which our terminology originates. The second row shows one example of a thin-film inductor in the pot-core class and two in the toroid class.

using two depositions of magnetic material "pot-core" designs, because, like a conventional pot-core transformer (Fig. 11(a)), they have magnetic material surrounding a coil (Fig. 11(c)). The designs in the class using two depositions of conductor are termed toroidal designs (Fig. 11(d) and 11(e)) because, like a conventional toroidal transformer (Fig. 11(b)), they have a coil surrounding a core.

A key consideration favoring the use of two magnetic layers is that many thin-film magnetic materials are anisotropic, and it is necessary to keep the direction of magnetic flux parallel to one axis [19]. The most common type thin-film "pot-core" geometry is the racetrack design (Fig. 11(c)), which uses magnetic material only on two sides to allow the use of anisotropic material with a consistent orientation. However, if the magnetic material is expensive to deposit, the need for two separate magnetic deposition steps may increase cost. Additionally, in a "pot-core" design, there are "magnetic vias" where flux transfers between the top magnetic layers and the bottom magnetic layers. This typically requires flux lines to cross through layers of a laminated magnetic material, resulting increased eddy current losses in this region [26–29], which can be one of the main contributions to the power loss [29].

Toroidal designs allow flux to travel purely in the plane of the film, avoiding problems with magnetic vias, and they can be produced with a single deposition of magnetic material. However, in toroidal designs the direction of flux is different in different regions. If a magnetic material with uniaxial anisotropy is used, the flux must be perpendicular to the favored hard-axis direction in some regions [25]. Although the size of that region can be minimized through the use of a rectangular geometry such as that shown in Fig. 11(e), the incorrectly oriented end regions may not contribute significantly to the performance of the inductor [30,31].

Similarly, if the magnetic structure in Fig. 1 were fabricated with the core in the plane of the substrate, deposited in one step, a magnetic material with strong anisotropy would not provide strong coupling between the phases. Thus, it was recognized early on that the "pot-core" category of topologies offered the best opportunity for microfabricted coupled inductors. The most commonly used configuration was first developed in a collaborative project

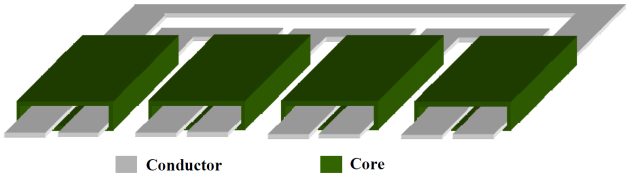

Figure 12: Schematic diagram of a microfabricated coupled inductor

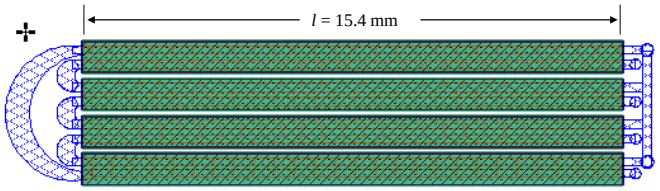

Figure 13: Layout of a microfabricated coupled inductor.

using a Dartmouth design shown in Figs. 12 and 13, fabricated in a process at the Tyndall National Institute in Ireland [12, 13], as an initial proof of concept. Subsequent fabrication in higher-performance processes has led to higher power density and efficiency [14, 15, 18, 28]. In once sense, this design may be thought of as the structure in Fig. 1 stretched out of the page, and with the lower plate of the core parallel to the substrate. However, uninterrupted top and bottom plates of conductive magnetic material lead to excessive eddy currents, and, as with the race-track inductor in Fig. 11(c), the core sections that enclose each winding window must be separated. The resulting configuration may be considered a set of two-winding transformers, each coupling two phases, with each phase connected through two such transformers directly coupling it to the two adjacent phases [18]. The details of the model are slightly different than the model discussed in Section 3: the inductance matrix is more sparse with zeros in some positions. However, general behavior and the design approach remain the same: the leakage inductance per phase determines the transient response. With that value fixed, the design goal is to maximize the coupling through the use of high-permeability materials with minimal air gaps. In the limit of high coupling, the

phase current ripple reduction γ approaches the output current ripple reduction Γ and the success of coupling can be evaluated in terms of the extent to which the coupling approaches that ideal.

Another approach to microfabricated inductors is to use the the magnetic structure in Fig. 1, fabricated with the core in the plane of the substrate and to overcome the anisotropy problem by depositing many layers of magnetic core material with the anisotropy orientation rotated 90° between layers [16], as had been previously applied to inductors [32, 33]. This principle allows high permeability for any flux direction, and enables strong coupling. A key disadvantage is that it required double the thickness of magnetic material as would be required if the material had isotropic high permeability.

Given the challenges inherent in using high-permeability magnetic material, another option is to simply use air-core inductors. However, without a magnetic core, structuring the coupling as in Fig. 1 and providing strong coupling is not feasible for more than two phases. The most practical ways to apply air-core coupling are thus to use only two phases or, within a system with a larger number of phases, to couple pairs of phases that are switched 180° out of phase. This has been applied commercially in some Intel designs, but the benefits are small [34]. One reason for this is that the limitation to two phases constrains the available benefit. However, as can be seen in Fig. 8, this isn't always a serious problem: when the duty ratio is sufficiently close to 0.5 the benefit of two-phase coupling can be nearly as good as the benefit with larger numbers of phases. The more important limitation is that without a high-permeability core, high magentizing inductance can only be achieved through the use of a large area current loop or more turns, in either case incurring higher winding loss. Another way to look at this is that a significant part of the advantage of the coupled inductor structure arises through the way that the dc fluxes cancel to avoid saturation in a high-permeability magnetic core. In an air-core inductor, there are no saturation effects and this benefit is irrelevant.

In summary, coupling two or more phases can offer advantages that are particularly useful in integrated implementations. Although coupling in air-core designs has successfully provided minor benefits, the most significant benefits occur with a high-permeabilty magnetic core. The most common design remains the extension of the "racetrack" inductor configuration to coupled inductors, first published in 2004, and shown in Figs. 12 and 13. However, an extension of the "toroidal" class of microfabricated designs has been applied by using laminated layers with alternating anisotropy.

5 Conclusions

Whether the magnetics are discrete or integrated, coupling between phases in a multiphase buck converter confers many advantages. With good design work, these benefits may be applied to specific attributes the designer wishes to improve, whether that includes cost, size, response time, and/or efficiency. The benefits result from both the circuit behavior and the effective utilization of the magnetic material, and thus the benefits are greatest when a high-permeability material is available.

It is shown that phase-current ripple reduction provided by coupling can be calculated with a simple equation in terms two parameters, Γ which quantifies the output ripple current reduction provided by multiphase interleaving, and β which quantifies the degree of coupling. This formulation simplifies design and analysis calculations, while also providing insight on origin of the coupling benefit.

Successful implementation of microfabricated coupled inductors for multiphase buck applications were reviewed. Air-core versions offer limited advantages through coupling, but two different general classes of magnetic-core geometries have been demonstrated to work well.

6 Acknowledgements

This work was partially supported by the the National Science Foundation under Award #1847365.

References

[1] B. A. Miwa, "Interleaved conversion techniques for high density power supplies," Ph.D. dissertation, Massachusetts Institute of Technology, 1992.

[2] C. Chang and M. A. Knights, "Interleaving technique in distributed power conversion systems," *IEEE Transactions on Circuits and Systems I: Fundamental Theory and Applications*, vol. 42, no. 5, pp. 245–251, May 1995.

[3] D. J. Perreault and J. G. Kassakian, "Distributed interleaving of paralleled power converters," *IEEE Transactions on Circuits and Systems I: Fundamental Theory and Applications*, vol. 44, no. 8, pp. 728–734, August 1997.

[4] X. Zhou, P.-L. Wong, P. Xu, F. C. Lee, and A. Q. Huang, "Investigation of candidate vrm topologies for future microproceossrs," *IEEE Trans. Power Electron*, vol. 15, November 2000.

[5] P.-L. Wong, P. Xu, P. Yang, and F. C. Lee, "Performance improvements of interleaving vrms with coupling inductors," *IEEE Trans. on Power Electron*, vol. 16, p. 4, 2001.

[6] J. Li, C. R. Sullivan, and A. Schultz, "Coupled inductor design optimization for fast-response low-voltage dc-dc converters," in *IEEE Applied Power Electronics Conference and Exposition*, vol. 2, 2002, pp. 817–823.

[7] A. M. Schultz and C. R. Sullivan, "Voltage converter with coupled inductive windings, and associated methods," 2002, US Patent 6,362,986.

[8] J. Li, A. Stratakos, C. R. Sullivan, and A. Schultz, "Using coupled inductors to enhance transient performance of multiphase buck converters," in *IEEE Applied Power Electronics Conference and Exposition*, vol. 2, 2004, pp. 1289–1293.

[9] P. Zumel, O. Garcia, J. A. Cobos, and J. Uceda, "Tight magnetic coupling in multiphase interleaved converters based on simple transformers," in *IEEE Applied Power Electron. Conf*, 2005.

[10] T. Schmid and A. Ikriannikov, "Magnetically coupled buck converters," in *IEEE Energy Conversion Congress and Exposition*, 2013, pp. 4948–4954.

[11] A. Ikriannikov, *The Benefits of the Coupled Inductor Technology*. Maxim Integrated Tutorial, 2014, vol. 5997.

[12] S. Prabhakaran, C. R. Sullivan, T. O'Donnell, M. Brunet, and S. Roy, "Microfabricated coupled inductors for DC-DC converters for microprocessor power delivery," in *2004 IEEE 35th Annual Power Electronics Specialists Conference (IEEE Cat. No. 04CH37551)*, vol. 6. IEEE, 2004, pp. 4467–4472.

[13] S. Prabhakaran, T. O'Donnell, C. R. Sullivan, M. Brunet, S. Roy, and C. O'Mathuna, "Microfabricated coupled inductors for integrated power converters," *Journal of magnetism and magnetic materials*, vol. 290, pp. 1343–1346, 2005.

[14] J. T. Dibene, P. Morrow, C. Park, H. W. Koertzen, and P. Zou, "A 400-amp fully integrated silicon voltage regulator with in-die magnetic coupled embedded inductors," in *Proc. Appl. Power Electron. Conf., Special Session on On-Die Voltage Regulators*, 2010.

[15] N. Sturcken, E. J. O'Sullivan, N. Wang, P. Herget, B. C. Webb, L. T. Romankiw, M. Petracca, R. Davies, R. E. Fontana, G. M. Decad *et al.*, "A 2.5-D integrated voltage regulator using coupled-magnetic-core inductors on silicon interposer," *IEEE Journal of Solid-State Circuits*, vol. 48, no. 1, pp. 244–254, 2013.

[16] R. P. Davies, C. Cheng, N. Sturcken, W. E. Bailey, and K. L. Shepard, "Coupled inductors with crossed anisotropy CoZrTa/SiO_2 multilayer cores," *IEEE Transactions on Magnetics*, vol. 49, no. 7, pp. 4009–4012, 2013.

[17] E. A. Burton, G. Schrom, F. Paillet, J. Douglas, W. J. Lambert, K. Radhakrishnan, and M. J. Hill, "FIVR—fully integrated voltage regulators on 4th generation Intel Core SoCs," in *2014 IEEE Applied Power Electronics Conference and Exposition-APEC 2014*. IEEE, 2014, pp. 432–439.

[18] Y. Kandeel and M. Duffy, "Comparison of coupled vs. non-coupled microfabricated inductors in 2 W 20 MHz interleaved buck converter," in *2019 IEEE Applied Power Electronics Conference and Exposition (APEC)*. IEEE, 2019, pp. 2638–2645.

[19] C. R. Sullivan, D. V. Harburg, J. Qiu, C. G. Levey, and D. Yao, "Integrating magnetics for on-chip power: A perspective," *IEEE Transactions on Power Electronics*, vol. 28, no. 9, pp. 4342–4353, 2013.

[20] C. Ó. Mathúna, N. Wang, S. Kulkarni, and S. Roy, "Review of integrated magnetics for power supply on chip (pwrsoc)," *IEEE Transactions on Power Electronics*, vol. 27, no. 11, pp. 4799–4816, 2012.

[21] C. R. Sullivan, B. A. Reese, A. L. F. Stein, and P. A. Kyaw, "On size and magnetics: Why small efficient power inductors are rare," in *2016 International Symposium on 3D Power Electronics Integration and Manufacturing (3D-PEIM)*, 2016, pp. 1–23.

[22] M. Chen and C. R. Sullivan, "Unified models for multiphase coupled inductors," Jun 2020. [Online]. Available: https://www.techrxiv.org/articles/preprint/Unifying_Models_for_Multiphase_Coupled_Inductors/12477269

[23] Y. Dong, "Investigation of multiphase coupled-inductor buck converters in point-of-load applications," Ph.D. dissertation, , Virginia Tech, 2009.

[24] D. Zhou, Y. Elasser, J. Baek, C. R. Sullivan, and M. Chen, *Inductance Dual Model and Control of Multiphase Coupled Inductor Buck Converter*. Aalborg, Denmark: IEEE Workshop on Control and Modeling of Power Electronics, 2020.

[25] C. R. Sullivan and S. R. Sanders, "Design of microfabricated transformers and inductors for high-frequency power conversion," *IEEE Transactions on Power Electronics*, vol. 11, no. 2, pp. 228–238, 1996.

[26] ——, "Measured performance of a high-power-density microfabricated transformer in a dc-dc converter," in *IEEE Power Electronics Specialists Conference (PESC)*, Jun. 1996, pp. 287–294.

[27] C. R. Sullivan, "Microfabrication of magnetic components for high frequency power conversion," Ph.D. dissertation, University of California, Berkeley, 1996.

[28] P. R. Morrow, C.-M. Park, H. W. Koertzen, and J. T. DiBene, "Design and fabrication of on-chip coupled inductors integrated with magnetic material for voltage regulators," *IEEE Transactions on Magnetics*, vol. 47, no. 6, pp. 1678–1686, 2011.

[29] D. V. Harburg, X. Yu, F. Herrault, C. G. Levey, M. G. Allen, and C. R. Sullivan, "Micro-fabricated thin-film inductors for on-chip power conversion," in *2012 7th International Conference on Integrated Power Electronics Systems (CIPS)*. IEEE, 2012, pp. 1–6.

[30] J. M. Wright, D. W. Lee, A. Mohan, A. Papou, P. Smeys, and S. X. Wang, "Analysis of integrated solenoid inductor with closed magnetic core," *IEEE Trans. Magn.*, vol. 46, pp. 2387–2390, Jun. 2010.

[31] Dok Won Lee, Kyu-Pyung Hwang, and Shan X. Wang, "Fabrication and analysis of high-performance integrated solenoid inductor with magnetic core," *IEEE Trans. Magn.*, vol. 44, no. 11, pp. 4089–4095, 2008.

[32] M. Frommberger, J. McCord, and E. Quandt, "Crossed anisotropy magnetic cores for integrated inductors," *Journal of magnetism and magnetic materials*, vol. 290, pp. 1487–1490, 2005.

[33] M. Frommberger, C. Schmutz, M. Tewes, J. McCord, W. Hartung, R. Losehand, and E. Quandt, "Integration of crossed anisotropy magnetic core into toroidal thin-film inductors," *IEEE Transactions on microwave theory and techniques*, vol. 53, no. 6, pp. 2096–2100, 2005.

[34] W. J. Lambert, M. J. Hill, K. Radhakrishnan, L. Wojewoda, and A. E. Augustine, "Package inductors for intel fully integrated voltage regulators," *IEEE transactions on components, packaging and manufacturing technology*, vol. 6, no. 1, pp. 3–11, 2015.